Adsorption of Spillover Hydrogen Atoms on Single-Wall Carbon Nanotubes

Frances H. Yang, Anthony J. Lachawiec, Jr., and Ralph T. Yang*

Department of Chemical Engineering, University of Michigan, Ann Arbor, Michigan 48109

Received: November 8, 2005; In Final Form: February 3, 2006

Spillover of hydrogen on nanostructured carbons is a phenomenon that is critical to understand in order to produce efficient hydrogen storage adsorbents for fuel cell applications. The spillover and interaction of atomic hydrogen with single-walled carbon nanotubes (SWNTs) is the focus of this combined theoretical and experimental work. To understand the spillover mechanism, very low occupancies (i.e., 1 and 2 H atoms adsorbed) on (5,0), (7,0), (9,0) zigzag (semiconducting) SWNTs and a (5,5) armchair (metallic) SWNT, with corresponding diameters of 3.9, 5.5, 7.0, and 6.8 Å, were investigated. The adsorption binding energy of H atoms depends on H occupancy, tube diameter, and helicity (or chirality), as well as endohedral (interior) vs exohedral (exterior) binding. Exohedral binding energies are substantially higher than endohedral binding energies due to easier sp^2-sp^3 transition in hybridization of carbon on exterior walls upon binding. A binding energy as low as −8.9 kcal/mol is obtained for 2H atoms on the exterior wall of a (5, 0) SWNT. The binding energies of H atoms on the metallic SWNT are significantly weaker (about 23 kcal/mol weaker) than that on the semiconductor SWNT, for both endohedral and exohedral adsorption. The binding energy is generally higher on SWNTs of larger diameters, while its dependence on H occupancy is relatively weak except at very low occupancies. Experimental results at 298 K and for pressures up to 10 MPa with a carbon-bridged composite material containing SWNTs demonstrate the presence of multiple adsorption sites based on desorption hysteresis for the spiltover H on SWNTs, and the experimental results were in qualitative agreement with the molecular orbital calculation results.

Introduction

The earliest report of hydrogen adsorption on single-walled carbon nanotubes (SWNTs)[1] generated experimental and theoretical interest in the use of nanostructured carbon materials for hydrogen storage, which has continued to increase as researchers attempt to deliver a viable material to meet the DOE target (of 6.5 wt % at ambient temperature). Various forms of carbon nanotubes,[2−11] graphite nanofibers,[12−17] and activated carbon and graphite[18−20] have been studied as potential hydrogen storage sorbents. The reported storage amounts have covered a wide range, and this subject remains controversial. A detailed review of the material structures, experimental techniques, and observed capacities is given elsewhere.[21]

A continuing effort in this area is the theoretical study in order to provide a rationale for the storage mechanism. These studies have been discussed in recent publications.[22−25] The majority of the theoretical studies were for the adsorption of hydrogen molecules in/on SWNTs[9,10,22,25−32] while studies on adsorption of H atoms are few.[25,31,33−36] For hydrogen adsorption on SWNT, classical statistical mechanics simulations on rigid SWNT models suggested that the energies of adsorption were below or near 1 kcal/mol. In the ab initio molecular dynamics simulations of Cheng et al., instantaneous distortion of the graphene structure on the tube was allowed (by using an empirical force field that depends on curvature), which led to some sp^3 character of carbon; and as a result, adsorption energies of more than 7 kcal/mol were obtained,[9,22,37] although some disagreements exist.[32,38,39] For adsorption of H atoms on SWNTs, the calculated adsorption energies were typically in the range of 50−70 kcal/mol for the high loadings that were studied.[25,31,33−36]

It has been suggested that most of the experimental data on significant amounts of hydrogen storage on carbon nanotubes involved dissociation of molecular hydrogen into hydrogen atoms followed by atomic hydrogen spillover, because the nanotube samples invariably contained residues of a transition metal;[40−41] and it was further suggested that catalysts should be introduced in order to achieve dissociation/spillover and consequently significant storage.[41] By using Pd/carbon as the dissociation catalyst, the storage amount on AX-21 carbon at 10 MPa and 25 °C was increased by a factor of 2.7 (to 2 wt %).[42]

As mentioned, the past simulations of atomic hydrogen adsorption on carbon nanotubes were performed at high loadings or occupancies. To understand the dissociation and spillover phenomenon, adsorption of H at low occupancies is a necessary path for storage and desorpion. In this work, ab initio molecular orbital calculations were performed for H atoms on SWNTs at very low occupancies (i.e., 1 and 2 H atoms). SWNTs of different diameters and chiralities (zigzag and armchair orientations) were employed. Moreover, dissociation/spillover experimental data on SWNTs with a Pt catalyst were performed and the results compared with the calculations.

Computational Details

We studied the chemisorption of atomic hydrogen on single-walled carbon nanotubes of different sizes: (5,0), (7,0), and (9,0) zigzag carbon nanotubes and (5,5) armchair carbon nanotube, with corresponding diameters of 3.9, 5.5, 7.0, and 6.8 Å. Of these SWNTs, the (5,5) armchair tube is a metal,

* Address correspondence to this author. E-mail: yang@umich.edu. Fax: (734) 764-7453.

10.1021/jp056461u CCC: $33.50
Published on Web 03/02/2006

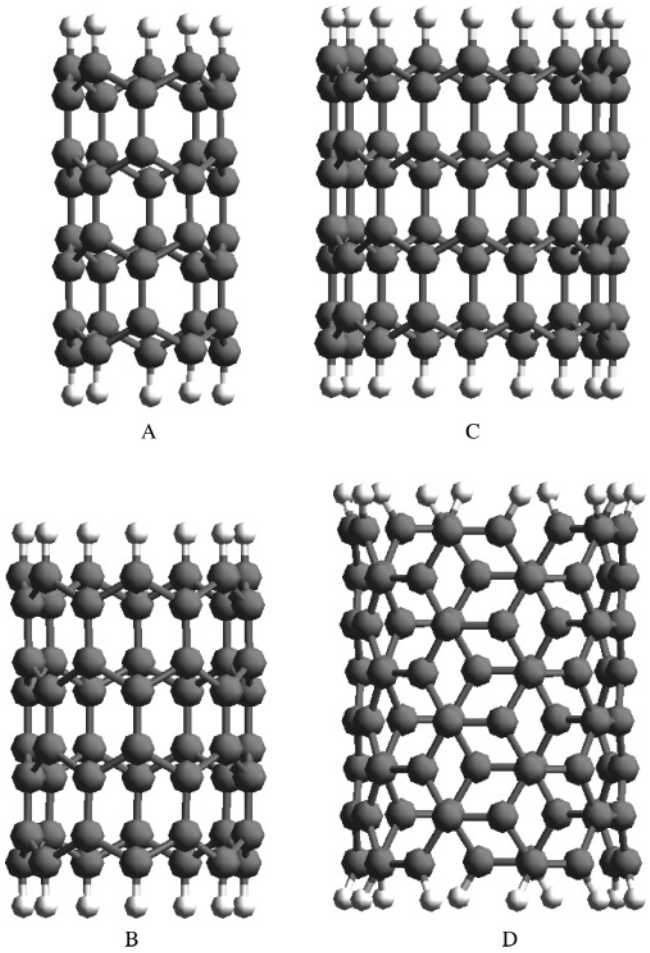

Figure 1. Carbon nanotube models: A = (5,0) CNT, B = (7,0) CNT, C = (9,0) CNT, and D = (5,5) CNT. The (5,5) CNT is metallic while the others are semiconductors. Small white balls are H.

while the others are semiconductors.[43] The bare carbon nanotube (CNT) models shown in Figure 1 have 40, 56, 72, and 80 carbon atoms with respectively 10, 14, 18, and 20 hydrogen atoms terminating the edge carbon atoms on the two open ends. In Figure 2, the CNT models are shown with one hydrogen atom adsorbed on the exterior wall, and in Figure 3, the CNT models are shown with one hydrogen atom adsorbed on the interior wall.

Since all the models we used here are still small enough for us to do molecular orbital calculations with the all-electron ab initio method, therefore for comparison purposes, we used the ab initio molecular orbital method as well as the Our own *N*-layered Integrated molecular Orbital and molecular Mechanics (ONIOM) method. We will compare the results obtained from both methods for their accuracies.

The ONIOM method was developed by Morokuma and coworkers[44−49] in the late 1990s; it is available in the Guassian98 package.[50] In the literature, it is also known as the quantum mechanics/molecular mechanics (QM/MM) mixed model used by Bauschlicher[34] and Froudakis.[35] In our ONIOM approach, the CNT model system is divided into two layers, each layer being calculated with a different method. A highly accurate molecular orbital method is applied to the most important part of the model system, i.e., around the center of a chemical reaction, and one less accurate molecular mechanics method is applied to the rest of the model system. In our CNT models, the area of interest is the area where hydrogen adsorbs on the sidewall of CNT. Geometry optimization and energy calculation are performed at the density functional theory (DFT)[50] level

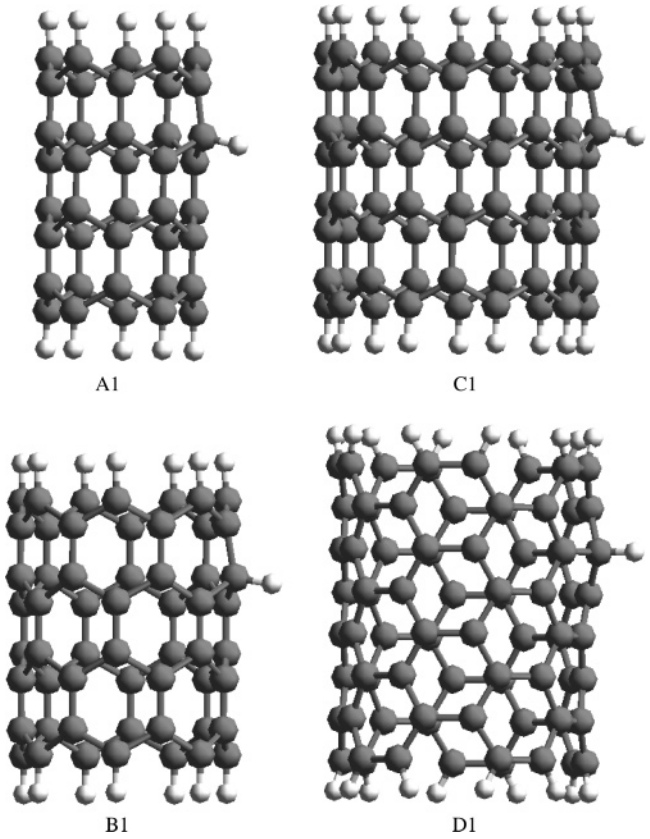

Figure 2. Models A1, B1, C1, and D1 with one hydrogen atom adsorbed on the exterior wall of CNTs. Small white balls are H.

with use of the basis set of 6-311G(d) or 6-31G(d,p). The remaining atoms on the CNT are performed at a lower level theory such as the Universal Force Field (UFF).[51,52] For example, in the case of (5,0) zigzag CNT, the system has 40 carbon atoms with 10 hydrogen atoms terminating the edge carbon atoms on two ends; only the hydrogen used for studying hydrogen adsorption and the carbon atom where the hydrogen is adsorbed on and nine other carbon atoms surrounding this carbon atom are part of the high level calculation, the rest of the CNT including 30 carbon atoms and 10 hydrogen atoms are part of the low level calculation, as shown in Figure 4, where atoms for high level calculation are shown in a lighter shade.

For the all-electron ab initio molecular orbital calculation, the Hartree−Fock (HF) method with the basis set of 3-21G(d) was used for geometric optimization, and the DFT method with the basis set of 6-31G(d) or 6-31G(d,p) was used for SCF energy calculations. The DFT method used is a hybrid method consisting of HF and DFT, known as the self-consistent hybrid (SCH) approach or B3LYP.[53−54] this is the combination of HF and Becke exchange[55] with the Lee−Yang−Parr (LYP) correlation potential.[56]

The bond energy of the CNT−hydrogen bond is determined by the expression:

$$E_{ads} = E_{CNT-H} - E_{CNT} - E_H$$

where E_{ads} is the hydrogen adsorption energy or C−H binding energy, E_{CNT-H} is the total energy of the CNT-H system, E_{CNT} is the total energy of the bare CNT, and E_H is the energy of the adsorbate or hydrogen atom. A higher E_{ads} corresponds to a stronger adsorption.

Results and Discussion

Geometry Optimizations. The optimized structures of (5,0), (7,0), and (9,0) CNTs with the ab initio molecular orbital

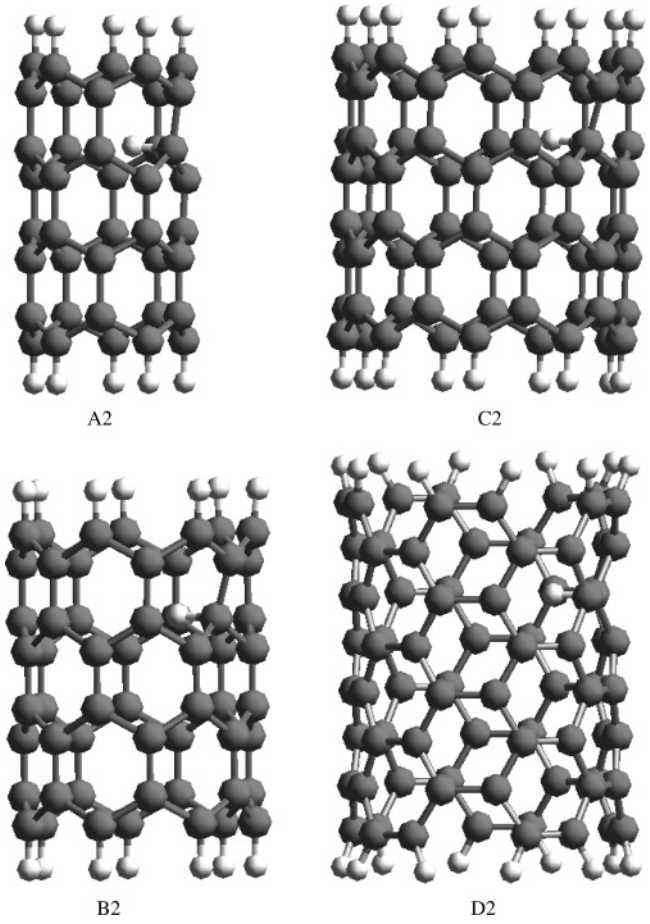

Figure 3. Models A2, B2, C2, and D2, with one hydrogen atom adsorbed on the interior wall of CNTs. Small white balls are H.

approach resulted in an average C−C bond length of 1.42 Å, whereas with the ONIOM approach, the average C−C bond length is close to 1.45 Å. These values are all in good agreement with the value of 1.42 Å for the C−C bond in β-graphite (most stable graphite). Upon a hydrogen atom adsorption on the exterior sidewall or the interior sidewall of the CNTs, a C−H bond was formed with a bond length of 1.1 Å in all cases, which is similar to the C−H bond length for the CH_4 molecule. Both the Ab initio approach and the ONIOM approach resulted in similar change of C−C bonds. In all CNT models, only the three adjacent C−C bonds increased in length, indicating weakening of these bonds; the rest of the C−C bonds were not affected much by the hydrogen adsorption. In the ab initio approach, the three adjacent bonds increased from 1.42 to 1.52 Å for the exterior wall and 1.50 Å for the interior wall. In the ONIOM approach, the three adjacent C−C bonds increased from 1.45 to 1.55 Å for the exterior wall and 1.51 Å for the interior wall. This increase in bond length is due to the change of hybridization of the carbon atom where the hydrogen atom is adsorbed. The hybridization changed from sp^2 to sp^3, thus the three adjacent C−C bonds changed from sp^2-sp^2 to sp^2-sp^3. The hydrogen atom on the exterior sidewall of the CNT pulls the three carbon atoms outward, enhancing sp^3 hybridization, while the binding of hydrogen−carbon inside the CNT pulls the three carbon atoms inward. In the latter case, although the sp^3 hybridization is also formed, but because it is geometrically unfavorable, some distortions are involved in the process. Therefore, the increase in C−C bond length is less for hydrogen on the interior wall. These structural differences for adsorption on the interior wall and the exterior wall are also clearly seen in their calculated energies of adsorption.

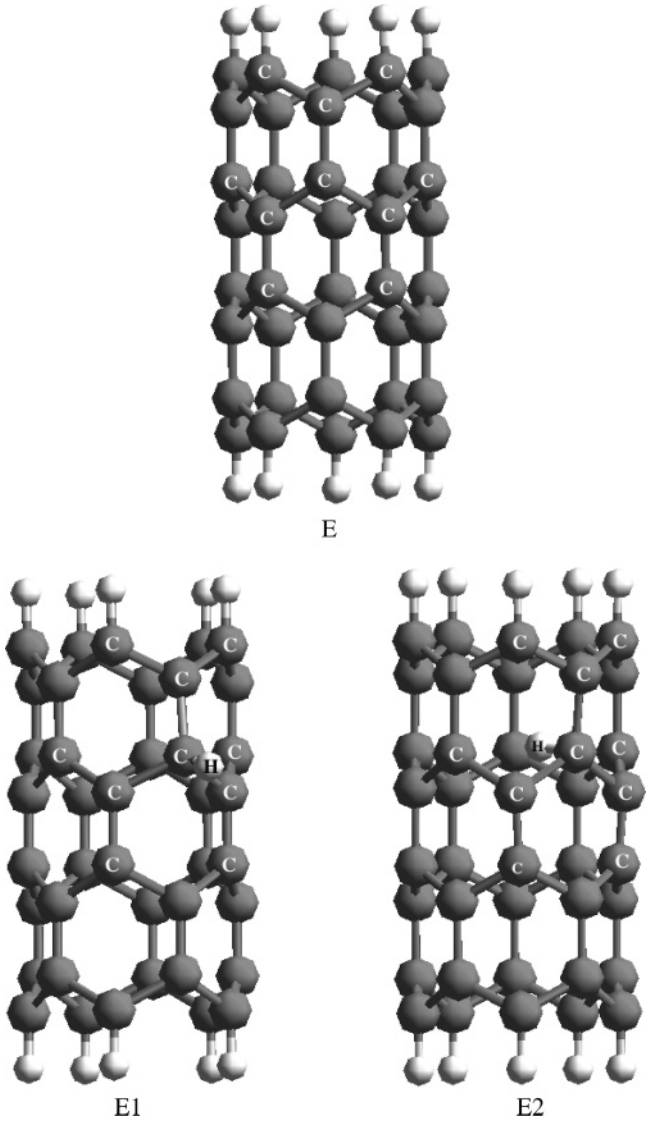

Figure 4. Carbon nanotube models for ONIOM study: E, (5,0) CNT in two layers; E1, one hydrogen atom adsorbed at the exterior tube wall of (5,0) CNT; E2, one hydrogen atom adsorbed at the interior tube wall of (5,0) CNT. For high-level calculations, carbon atoms are labeled "C" and hydrogen atom is labeled "H". Small white balls are H.

TABLE 1: Calculated Energy of Chemisorption, E_{ads}, of 1 Hydrogen Atom Adsorbed on the Exterior Wall

model	ab initio E_{ads} (kcal/mol)	ONIOM E_{ads} (kcal/mol)
A1 (5,0) semiconductor	−85.1	−85.0
B1 (7,0) semiconductor	−92.5	−89.8
C1 (9,0) semiconductor	−95.0	−94.1
D1 (5,5) metal	−72.3	−92.8

Adsorption Energy. The calculated hydrogen adsorption energies for one hydrogen atom adsorbed on the exterior sidewall of CNTs for both ab initio and ONIOM approaches are summarized in Table 1. The calculated hydrogen adsorption energies for one hydrogen atom adsorbed on the interior sidewall of CNTs for both ab initio and ONIOM approaches are summarized in Table 2.

The results show clearly that adsorption has a strong dependence on both tube diameter and helicity or chirality.

Hydrogen Adsorption on the Exterior Wall of CNTs (Exohedral Adsorption). The optimized geometries for one hydrogen atom adsorbed on the exterior walls of the 4 SWNTs

TABLE 2: Calculated Energy of Chemisorption, E_{ads}, of 1 Hydrogen Atom Adsorbed on the Interior Wall

model	ab initio E_{ads} (kcal/mol)	ONIOM E_{ads} (kcal/mol)
A2 (5,0) semiconductor	−16.6	−27.2
B2 (7,0) semiconductor	−47.8	−53.6
C2 (9,0) semiconductor	−59.1	−53.9
D2 (5,5) metal	−36.7	−70.1

are shown in Figure 2. In Table 1, we can see that in the case of zigzag CNTs, the calculated energies of chemisorption of hydrogen on the exterior wall by the ab initio approach are very close to the values by the ONIOM approach. In both cases, as the size of the CNT increases, the energy of chemisorption also increases. It increases from −85 kcal/mol for (5,0) CNT, to around −90 kcal/mol for (7,0) CNT, and close to −95 kcal/mol for (9,0) CNT. These values are rather close to −99.5 kcal/mol, the C−H bond energy of the CH_4 molecule. However, in case of the (5,5) CNT or armchair CNT, which is *metallic*, the calculated value from the ab initio approach is much lower than that from the ONIOM approach, that is, almost 20 kcal/mol less. This discrepancy shows that in the *metallic* (5,5) CNT, the distant-neighbor carbon atoms have more influence on the carbon that is being bonded. In this case, the ab initio results are more accurate.

Since the size of (5,5) CNT (metal) is similar to that of (9,0) CNT (semiconductor), we would expect them to have similar C−H bond energies, which is true in the ONIOM approach but not in the ab initio approach. This result shows that the chemisorption bond on the metallic SWNT is significantly weaker (about 23 kcal/mol weaker) than that on the semiconductor SWNT. We also noted that calculated C−H bond energies for the metallic CNT are rather sensitive to the basis set that one uses in the ab initio approach, which is not the case for the semiconductor CNTs. It is interesting to note that by using an empirical curvature-dependent force field, Cheng et al. observed that the adsorption energies depended rather strongly on the tube diameter but the dependence (if any) was much weaker on the tube chirality.[57]

Hydrogen Adsorption on the Interior Wall of CNTs (Endohedral Adsorption). The optimized geometries for one hydrogen atom adsorbed on the interior walls of the 4 SWNTs are shown in Figure 3, and the binding energies are given in Table 2. From Table 2, it is noted that the hydrogen adsorption energy on the interior wall for both approaches is much lower than the hydrogen adsorption energy on the exterior wall. This is consistent with the geometry optimization results discussed above. Distortions on the sidewalls of the CNTs cause them to be less stable, and consequently result in lower C−H binding energies. As the CNT diameter increases, the amount of distortion decreases, therefore the C−H binding energy increases with tube diameter. The difference in the calculated values for hydrogen adsorption on the interior walls is much higher between the two approaches compared to that of the exterior wall, again a bigger difference is noted for the metallic CNT. From Tables 1 and 2, we conclude that the C−H binding energy is much lower on the interior sidewall, and it increases with the size of CNT.

The strong dependence of adsorption energy on the chirality of the CNT is again seen for endohedral adsorption. Interestingly, the chemisorption bond on the metallic SWNT is again weaker by about 23 kcal/mol than that on the semiconductor SWNT (Table 2).

Adsorption of Two or More Hydrogen Atoms on the Exterior Walls of CNTs. When two hydrogen atoms are bonded to the exterior sidewalls of CNTs, we compare the two cases where they attach to either two adjacent carbons or two alternate carbons. We did calculations using only the ab Initio approach for two hydrogen atoms on (5,0) CNT and (9,0) CNT. Figure 5 shows the optimized geometries for two H atoms bonded to the (5,0) CNT and Figure 6 shows that for the (9,0) CNT. The adsorption binding energies are listed in Table 3. As one can see when two hydrogen atoms are placed adjacent to each other, due to crowding effect, the binding energies become less than when two hydrogen atoms are placed in the alternate positions. Moreover, the binding energies for two hydrogen atoms are higher in (5,0) CNT than (9,0) CNT.

In the case of (5,0) CNT, we also performed ab initio calculations on an increasing number of hydrogen atoms on the exterior wall. It was found that the average energy of chemisorption for 10 hydrogen atoms decreased to −66 kcal /mol. This is about 33% coverage of hydrogen atoms on the exterior wall, and finally for 15 hydrogen atoms, which is 50% coverage, the average value decreased to −60 kcal/mol. This last value is very close to those reported in the literature. Lee and coworkers[58,59] reported C−H binding energy of −2.65 eV or −61 kcal/mol by performing density functional calculations of hydrogen storage on the exterior walls of (5,5) and (10, 10) single-walled carbon nanotubes. Bauschlicher[35] reported −57 kcal/mol for the average C−H binding energy of 50% coverage for a (10,0) CNT (using the ONIOM approach), and average binding energies of −51.3 kcal/mol for 100% occupancy and ca. −60 kcal/mol for 50% occupancy for a (9,0) CNT, all on the exterior walls of the nanotubes.[36] The CNTs used by Bauschlicher were capped at both ends, which obviously would lower the binding energies for H because fewer C−C bond distortions would be allowed in the capped CNTs.

Adsorption of Two Hydrogen Atoms on the Interior Walls of CNTs. In Table 4, similar calculation results are shown for two hydrogen atoms bonded to the interior sidewalls. The energies diminished substantially when compared to those on the exterior wall. Here again, due to crowding effects, the binding energies for the adjacent atoms are less than that of the alternate atoms. Also, as expected, the (5,0) CNTs are less stable than the (9,0) CNTs, and consequently, the binding energies are lower on the (5,0) CNT.

Notably, the binding energies are only −8.9 kcal/mol (adjacent) and −11.1 kcal/mol (alternate) for two H atoms bonded to the interior wall of the (5,0) CNT. These H atoms can be readily desorbed at room temperature.

On Flat Graphene. The effects of curvature cannot be addressed without specifying whether the adsorption is exohedral or endohedral. Nonetheless, a comparison with adsorption on flat graphene should provide further insight on the curvature effects. Thus, ab initio molecular orbital calculations for four graphene models were also included in this study. A planar graphene model G with 44 carbon atoms and 14 peripheral hydrogens, model G1 with one hydrogen adsorbed on the flat surface of G, model G2 with two hydrogen atoms adsorbed on two alternate carbons, and model G3 with two hydrogens adsorbed on two adjacent carbons are shown in Figure 7. The calculated energies of chemisorption, E_{ads}, on graphene model G are summarized in Table 5. The graphene model G is very close in size to the (5,0) CNT model A; yet the energy of adsorption for one hydrogen in G1 is almost half that of (5,0) CNT model A1 when hydrogen is on the exterior wall, but almost twice that of model A2 when hydrogen is on the interior wall. However, the energy for 1 H on graphene (of −43.3 kcal/mol) being exceeded by two cases of 1 H on the exterior walls

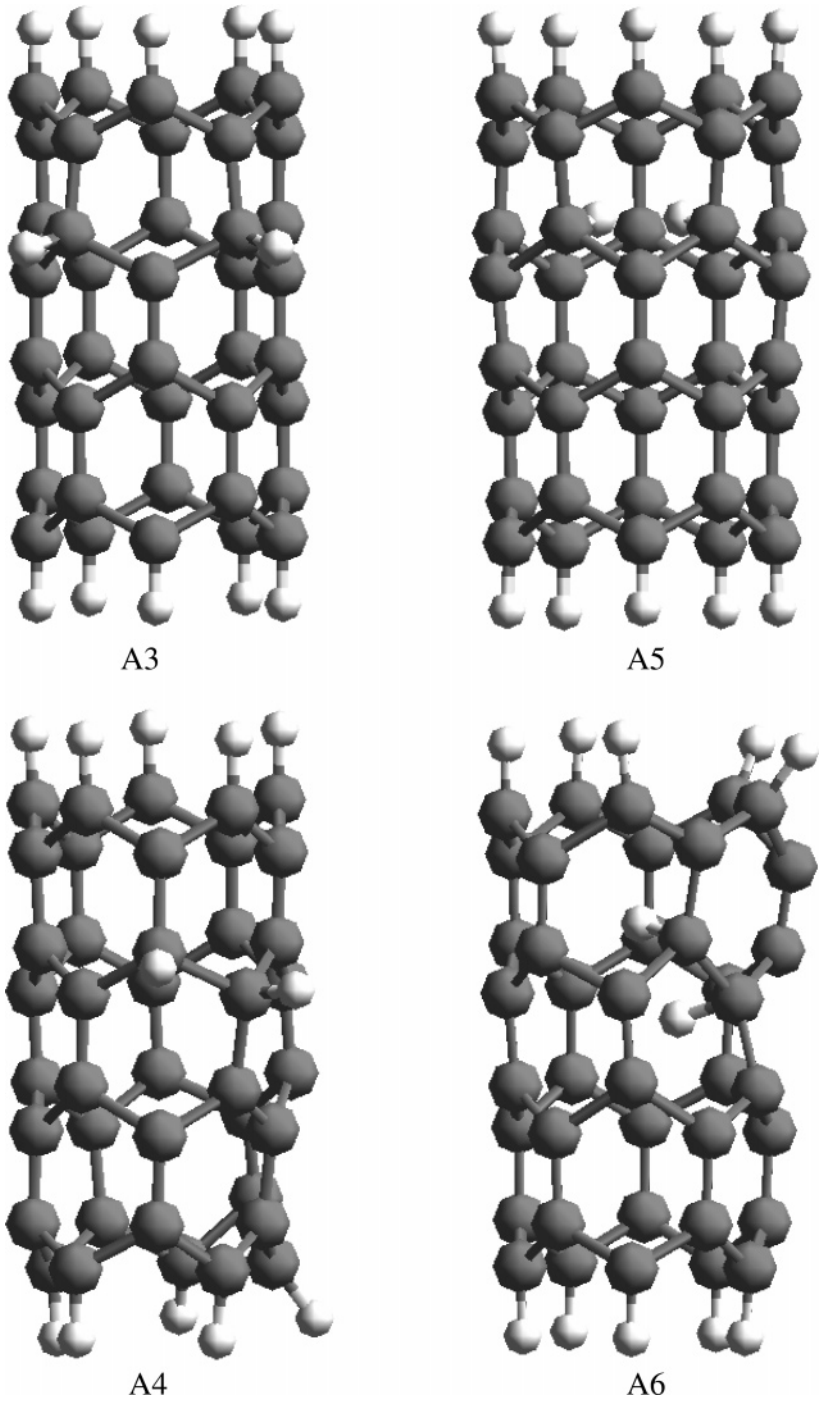

Figure 5. (5,0) CNTs with two hydrogen atoms adsorbed on the sidewall: A3, 2 alternate H's on the exterior wall; A4, 2 adjacent H's on the exterior wall; A5, 2 alternate H's on the interior wall; and A6, 2 adjacent H's on the interior wall. Small white balls are H.

of (7,0) and (9,0) tubes (Table 2) is rather unexpected. A possible reason could be the limited sizes of the SWNT models.

When two hydrogen atoms are adsorbed on the graphene, model G2 with the alternate hydrogens has a calculated binding energy of −34.3 kcal/mol, and G3 with the adjacent hydrogens has a lower binding energy of −28.7 kcal/mol. Comparing them to the binding energies of the (5,0) CNT models with two hydrogen atoms, one can see that for both alternate and adjacent hydrogens, the graphene energy value always lies between that of the exterior wall and that of the interior wall. The curvature effect for H_2 adsorption as discussed by Okamoto and co-workers[60] in their work is seen here on the exterior sidewall, and it is in the opposite direction on the interior wall.

Comparison of the Two Methods. As the CNT sizes increase, the computational time for the ab initio approach increases substantially, and is much more than that of the ONIOM approach; but the results from the two approaches are rather comparable in most cases. Even though the ONIOM approach requires less computational time, it requires more time to set up the input files, and convergence failures for the output files occurred more frequently. Therefore, the ab initio method should be the preferred method, especially when we need to calculate hydrogen adsorption for more than one hydrogen atom.

Experimental Section

Spillover of atomic hydrogen from a dissociation source to a receptor can allow the adsorbate to access sites that normally

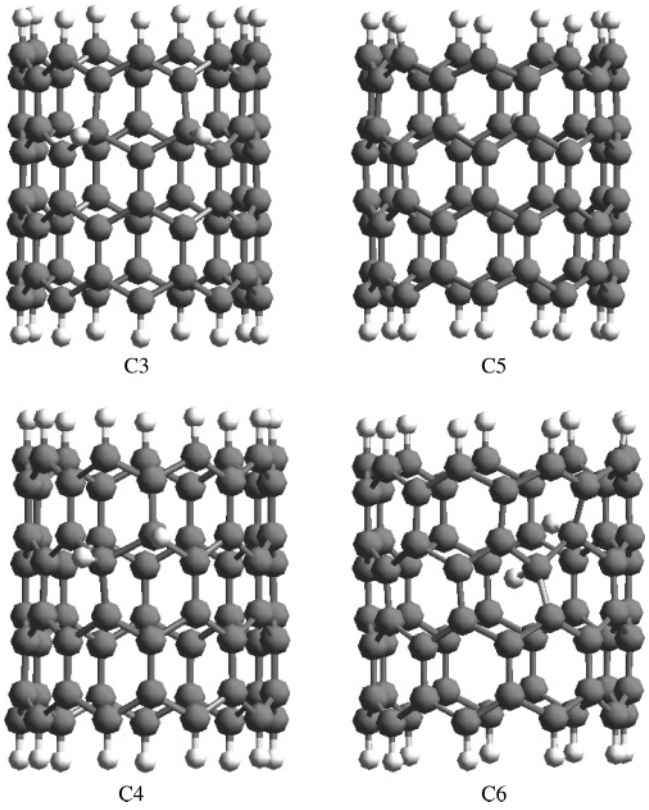

Figure 6. (9,0) CNTs with two hydrogen atoms adsorbed on the sidewall: C3, 2 alternate H's on the exterior wall; C4, 2 adjacent H's on the exterior wall; C5, 2 alternate H's on the interior wall; and C6, 2 adjacent H's on the interior wall. Small white balls are H.

TABLE 3: Calculated Energy of Chemisorption, E_{ads}, of 2 Hydrogen Atoms Adsorbed on the Exterior Wall

model	ab initio E_{ads} (kcal/mol)
A3 (5,0) alternate	−74.6
A4 (5,0) adjacent	−66.6
C3 (9,0) alternate	−66.9
C4 (9,0) adjacent	−51.4

TABLE 4: Calculated Energy of Chemisorption, E_{ads}, of 2 Hydrogen Atoms Adsorbed on the Interior Wall

model	ab initio E_{ads} (kcal/mol)
A5 (5,0) alternate	−11.1
A6 (5,0) adjacent	−8.9
C5 (9,0) alternate	−27.1
C6 (9,0) adjacent	−18.4

would be precluded from adsorption because of their physical configuration or, as the theoretical component of this study indicates, modification of the energetics associated with diffusion and sorption. The presence of strongly bound hydrogen that is not reversibly adsorbed, producing a hysteresis in the isotherm, is evidence of more than one type of sorption site and a corresponding binding energy.[61] Figure 8 depicts the spillover mechanism proposed for a material consisting of a hydrogen dissociation source (platinum particle on active carbon) and a receptor (SWNT). The carbon bridges formed between the source and receptor are proposed to aid in the diffusion process required for secondary spillover. As noted in previous work,[42] the method to form carbon bridges may also enhance the contact of the platinum particle with the active carbon support (though not depicted here) and thus enhance primary spillover. The presence of hydrogen atoms due to

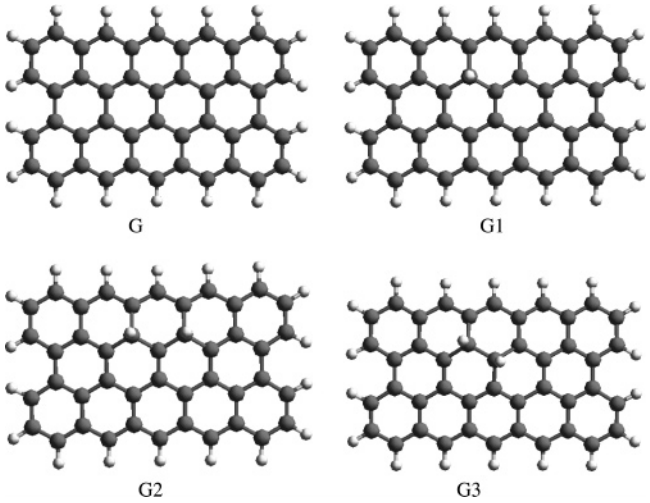

Figure 7. Graphene models: G, bare graphene; G1, with one hydrogen atom adsorbed; G2, with 2 adjacent hydrogen atoms adsorbed; and G3, with two alternate hydrogen atoms adsorbed. Small white balls are H.

TABLE 5: Calculated Energy of Chemisorption, E_{ads}, on Graphene Model G

model	ab initio E_{ads} (kcal/mol)
G1 with 1 H	−43.3
G3 with 2 H alternate	−34.3
G2 with 2 H adjacent	−28.7

dissociation spillover makes this system an interesting one for study as part of the combined theoretical and experimental effort.

Synthesis of Materials and Adsorption Measurements. To demonstrate the existence of multiple types of hydrogen adsorption sites present in SWNTs, volumetric adsorption data were collected at pressures from 0.1 to 10 MPa at 298 K. The apparatus and measurement technique were identical with those used for a previous study in this laboratory.[42] Figure 9 shows a schematic of the custom-built Sievert's apparatus. The SWNTs used in this study were produced by catalytic decomposition of methane on an iron catalyst supported on a hybrid alumina-silica support, as described by Cassel et al.[62] The purification procedure and residual metals analysis was identical with that of SWNTs used in a prior study.[42] The purified SWNTs had an estimated BET surface area of 1200 m^2/g with a peak in the pore size distribution at 15.5 Å measured by the Horvath−Kawazoe method for cylindrical pores. These SWNTs have limited ability for hydrogen dissociation and they are capable of receiving spillover hydrogen atoms when used as a receptor.

A composite material was synthesized by using SWNTs as a receptor and a spillover source bound to it by pyrolysis of a hydrocarbon precursor. The source of hydrogen atoms for spillover was a commercially available catalyst consisting of 5 wt % platinum supported on active carbon (Strem Chemicals, Inc.). Carbon bridges between the source and receptor were formed with the addition of certified ACS reagent grade sucrose (Fisher Scientific) to a physical mixture of the components. The crystalline sucrose was ground for 30 min into a fine powder before addition. The receptor/precursor/source ratio was fixed at 8:1:1 based on the empirical measurements of precursor carbonization using a thermogravimetric analyzer (TGA); thus, the bridges altered the amount of receptor compared to the simple physical mixture but not the source. The receptor/source physical mixture was ground with the precursor for 30 min. This material was transferred to a tubular reactor and heated in flowing helium with a temperature program designed to first

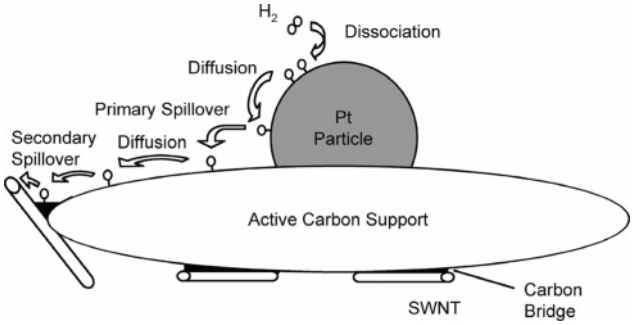

Figure 8. Proposed mechanism for primary and secondary spillover on a carbon bridged composite.

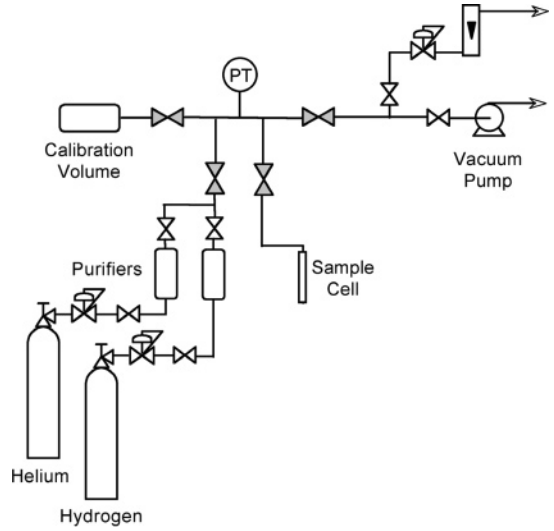

Figure 9. Sievert's apparatus to measure high-pressure hydrogen isotherms. Shaded valves have high-pressure bellows seals.

melt the precursor, allowing it to fill the interstices between the source and receptor, and then fully carbonize the precursor to form bridges. The temperature program was based on literature data for sucrose pyrolysis[63,64] and empirical measurements performed with a TGA. For the sucrose precursor, the temperature was increased at 1 deg/min to 463 K (just above the melting point, 458 K) and held for 3 h. In the carbonization step, the temperature was increased at 1 deg/min to 723 K and held for 5 min and then at 10 deg/min to 873 K. The initial slow-temperature ramp was designed to eliminate violent spattering and bubbling that might occur in the fluid during a rapid temperature ramp prior to carbonization. The material was cooled to room temperature in helium and stored for further pretreatment and hydrogen adsorption measurements.

Approximately 300 mg of each sample was used for high-pressure isotherm measurements. The volumetric apparatus was calibrated at 298 K with $LaNi_5$ powder (Cerac, Inc.) to ensure the accuracy of the instrument and calculation method. Each sample was pretreated at 1 Pa (7.5×10^{-3} Torr) and 673 K for 8 h in situ to the measurement apparatus prior to isotherm measurements. Ultrahigh purity hydrogen (99.999%) and helium (99.999%) were obtained from Cryogenic Gases (Detroit, MI) and used for all pretreatments and measurements. Molecular Sieve 3A purifiers were used on each gas stream to ensure purity was maintained in all experiments.

Experimental Results

The high-pressure hydrogen adsorption isotherm at 298 K was measured for the Pt−C catalyst and is presented in Figure 10. As the figure indicates, there is a hysteresis loop present for this system. This is due to spillover of atomic hydrogen that has dissociated on platinum particles and diffuses to the active carbon support. This type of spillover is primary spillover since the platinum particle is in direct contact with the carbon support. Since the catalyst is only a fraction of the bridged material, the contribution of the hydrogen adsorbed to the metal and carbon components of the catalyst is relatively minor.

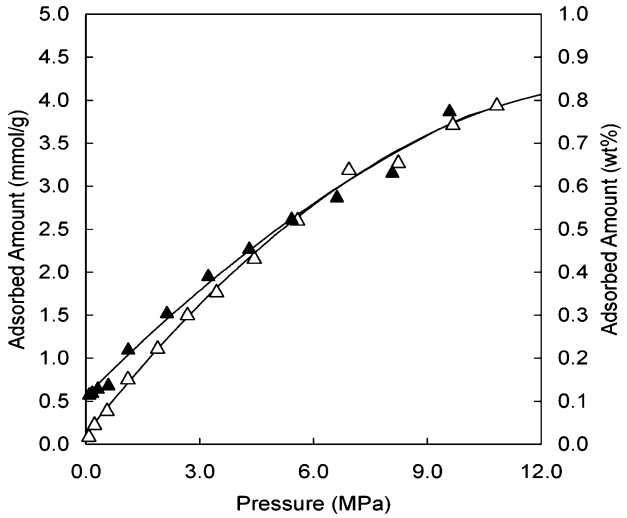

Figure 10. Hydrogen adsorption isotherm for Pt−C catalyst (spillover source) at 298 K. Filled symbols indicate desorption.

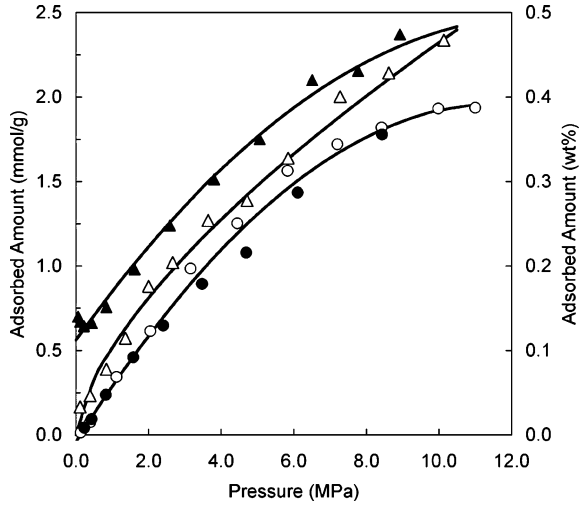

Figure 11. High-pressure hydrogen isotherms at 298 K for SWNT and spillover receptor: triangles, SWNT adsorption; circles, SWNT/Pt−C/carbon bridge (8:1:1) adsorption. Filled symbols indicate desorption.

Hydrogen isotherms at 298 K are presented in Figure 11 for SWNT and the SWNT/Pt−C/carbon bridge (8:1:1) mixture. The composite material demonstrates an enhancement of about 20% in hydrogen adsorption over the entire pressure range. This enhancement was not as great as that observed for an AX-21 receptor and a Pd−C source in previous work.[42] This could be due to the difference in the metallic component of the spillover source and would be an interesting subject of further study. The bridged material does, however, demonstrate a hysteresis in the desorption isotherm, which is absent for the pure SWNT isotherm. Comparing Figures 10 and 11 and considering the relatively small fraction of the Pt−C catalyst in the mixture, one notes that the observed hysteresis in the bridged material cannot be solely due to the Pt−C component. Thus, the presence of a hysteresis loop for the composite indicates that spillover

hydrogen, in the form of atoms, has accessed higher energy sites compared to those present in the pure SWNTs. This hydrogen is not readily desorbed at 0.1 MPa and 298 K while the hydrogen that occupies the lower energy sites is reversibly sorbed. To fully desorb the hydrogen at 298 K, the sample must be placed under full vacuum (1 Pa) for at least 12 h or heated to at least 423 K. This desorption behavior is consistent with a bond energy of the order of 10 kcal/mol.[39] That the adsorbed hydrogen was fully desorbed under the above-mentioned conditions was shown by the second adsorption step, which was essentially identical with the first adsorption isotherm.[42] The behavior of the bridged material is indicative of secondary spillover of H atoms from the Pt catalyst to the SWNTs. The physical bridge apparently promotes the diffusion of atomic hydrogen from the active carbon catalyst support (source) to the receptor. On the receptor, the hydrogen atoms access different adsorption sites compared to molecular hydrogen, and the binding energies of the atomic hydrogen on SWNT were sufficiently high as evidenced by the apparent hysteresis (at pressures down to 0.1 MPa). This result is in qualitative agreement with the molecular orbital calculation results.

On the basis of the molecular orbital results, the following path for desorption of the spiltover hydrogen is envisioned. Hydrogen is known to spillover, i.e., readily undergo surface diffusion at ambient temperature. This is also clearly seen in the experimental data shown in this work. Cheng et al.,[38] in their ab initio molecular dynamic simulations of hydrogen on single-walled nanotubes, showed rapid exchange of partially chemisorbed hydrogen between the interior wall and the exterior wall. For desorption of molecular hydrogen that requires desorption activation energy below 10−15 kcal/mol, desorption can take place readily at room temperature.[32,39]

On the basis of the results of this work, it is entirely possible to visualize a path by which molecular hydrogen is desorbed from a SWNT upon depressurization, starting from nearly full occupancy of hydrogen atoms on the SWNT (i.e., H/C $\sim$ 1). A few hydrogen atoms on the interior sites of the SWNT desorb first. The binding energies on these few interior sites are low, e.g., of the order of 10−15 kcal/mol. Since adsorbed hydrogen atoms are mobile and interior−exterior exchange is possible, these interior sites continue to serve as the sites to which hydrogen atoms migrate and from which hydrogen is desorbed as molecular hydrogen. Since there are a number of such patches of desorption sites, a broad desorption peak would be possible during temperature programmed desorption as observed by Dillon et al.[1] When a metal catalyst is present, the bond energy of hydrogen on metal can be low, e.g., 18 kcal/mol for H_2 on Pt. For such a system, desorption by reverse spillover where the metal surface serves as the desorption site is entirely possible. Through such desorption paths, reversibility of the hydrogen adsorption (and desorption) isotherm is expected and is indeed observed.[42]

Acknowledgment. The authors acknowledge the support of the U.S. Department of Energy (Lead: National Renewable Energy Laboratory) for this work under contract DE FC36 05 GO15078.

References and Notes

(1) Dillon, A. C.; Jones, K. M.; Bekkedahl T. A.; Kiang, C. H.; Bethune, D. S.; Heben, M. J. *Nature* **1997**, *386*, 377−379.

(2) Ye, Y.; Ahn, C. C.; Witham, C.; Fultz, B.; Liu, J.; Rinzler, A. G.; Colbert, D.; Smith, K. A.; Smalley, R. E. *Appl. Phys. Lett.* **1999**, *74*, 2307−2309.

(3) Wang, Q.; Johnson, J. K. *J. Phys. Chem. B* **1999**, *103*, 277−281.

(4) Liu, C.; Fan, Y. Y.; Liu, M.; Cong, H. T.; Cheng, H. M.; Dresselhaus, M. S. *Science* **1999**, *286*, 1127−1129.

(5) Chen, P.; Wu, X.; Lin, J.; Tan, K. L. *Science* **1999**, *285*, 91−93.

(6) Yang, R. T. *Carbon* **2000**, *38*, 623−626.

(7) Dillon, A. C.; Heben, M. J. *Appl. Phys. A* **2001**, *72*, 133−142.

(8) Tibbetts, G. G.; Meisner, G. P.; Olk, C. H. *Carbon* **2001**, *39*, 2291−2301.

(9) Cheng, H. S.; Pez, G. P.; Cooper, A. C. *J. Am. Chem. Soc.* **2001**, *123*, 5845−5486.

(10) Simonyan, V. V.; Johnson, K. J. *J. Alloys Compd.* **2002**, *330*, 659−665.

(11) Lueking, A.; Yang, R. T. *J. Catal.* **2002**, *206*, 165−168.

(12) Chambers, A.; Park, C.; Baker, R. T. K.; Rodriguez, N. M. *J. Phys. Chem. B* **1998**, *102*, 4253−4256.

(13) Ahn, C. C.; Ye, Y.; Ratnakumar, B. V.; Witham, C.; Bowman, R. C.; Fultz, B. *Appl. Phys. Lett.* **1998**, *73*, 3378−3380.

(14) Park, C.; Anderson, P. E.; Chambers, A.; Tan, C. D.; Hidalgo, R.; Rodriguez, N. M. *J. Phys. Chem. B* **1999**, *103*, 10572−10581.

(15) Gupta, B. K.; Srinivastava, O. N. *Int. J. Hydrogen Energy* **2001**, *26*, 857−862

(16) Browning, D. J.; Gerrard, M. L.; Lakeman, J. B.; Mellor, I. M.; Mortimor, R. J.; Turpin, M. C. *Nano Lett.* **2002**, *2*, 201−205.

(17) Lueking, A. D.; Yang, R. T.; Rodriguez, N. M.; Baker, R. T. K. *Langmuir* **2004**, *20*, 714−721.

(18) Chahine, R.; Bose, T. K. *Int. J. Hydrogen Energy* **1994**, *19*, 161−164.

(19) Lamari, M.; Aoufi, A.; Malbrunot, P. *AIChE J.* **2000**, *46*, 632−646.

(20) Orimo, S.; Meyer, G.; Fukunaga, T.; Züttel, A.; Schlapbach, L.; Fujii, H. *Appl. Phys. Lett.* **1999**, *75*, 3093−3095.

(21) Yang, R. T. *Adsorbents*: *Fundamentals and Applications*; Wiley: New York, 2003; pp 305−321.

(22) Cheng, H.; Pez, G.; Kern, G.; Kress, G.; Hafner, J. *J. Phys. Chem. B* **2001**, *105*, 736−742.

(23) Meregalli, V.; Parrinello, M. *Appl. Phys. A* **2001**, 72, 143−146.

(24) Froudakis, G. E. *J. Phys.*: *Condens. Matter* **2002**, *14*, R453−R465.

(25) Alonso, J. A.; Arellano, J. S.; Molina, L. M.; Rubio, A.; Lopez, M. J. *IEEE Trans. Nanotechnol.* **2004**, *3*, 304−310.

(26) Wang, Q.; Johnson, J. K. *J. Phys. Chem. B* **1999**, *103*, 4809−4813.

(27) Wang, Q.; Johnson, J. K. *J. Chem. Phys.* **1999**, *110*, 577−586.

(28) Simonyan, V. V.; Diep, P.; Johnson, J. K. *J. Chem. Phys.* **1999**, *111*, 9778−9783.

(29) Rzepka, M.; Lamp, P.; de la Casa-Lillo, M. A. *J. Phys. Chem. B* **1998**, *102*, 10894−10898.

(30) Williams, K. A.; Eklund, P. C. *Chem Phys. Lett.* **2000**, *320*, 352−358.

(31) Lee, S. M.; An, K. H.; Lee, Y. H.; Seifert, G.; Frauenheim, T. *J. Am. Chem. Soc.* **2001**, *123*, 5059−5063.

(32) Li, J.; Furuta, T.; Goto, H.; Ohashi, T.; Fujiwara, Y.; Yip, S. *J. Chem. Phys.* **2003**, *119*, 2376−2385.

(33) Bauschlicher, C. W. *Chem. Phys. Lett.* **2000**, *322*, 237−241.

(34) Bauschlicher, C. W. *Nano Lett.* **2001**, *1*, 223−226.

(35) Froudakis, G. E. *Nano Lett.* **2001**, *1*, 179−182.

(36) Bauschlicher, C. W.; So, C. R. *Nano Lett.* **2002**, *2*, 337−341.

(37) Kostov, M. K.; Cheng, H.; Cooper, A. C.; Pez, G. P. *Phys. Rev. Lett.* **2002**, *89*, 146105-1−146105-4.

(38) Cheng, H.; Cooper, A. C.; Pez, G. P. *J. Chem. Phys.* **2004**, *120*, 9427−9429.

(39) Li., J.; Yip, S. *J. Chem. Phys.* **2004**, *120*, 9430−9432.

(40) Yang, F. H.; Yang, R. T. *Carbon* **2002**, *40*, 437−444.

(41) Zhao, Y.; Kim, Y.-H.; Dillon, A. C.; Heben, M. J.; Zhang, S. B. *Phys. Rev. Lett.* **2005**, *94*, 155504-1−155504-4.

(42) Lachawiec, A. J., Jr.; Qi, G. S.; Yang, R. T. *Langmuir* **2005**, *21*, 11418−11424.

(43) Louie, S. G. Electronic Properties, Junctions, and Defects of Carbon Nanotubes. In *Carbon Nanotubes*; Dresselhaus, M. S., Dresselhaus, G., Avouris, P., Eds.; Topics in Appl. Phys. No. 80; Springer-Verlag: Heidelberg, Germany, 2001; pp 113−146.

(44) Svensson, M.; Humbel, S.; Froese, R. D. J.; Matsubara, T.; Sieber, S. N.; Morokuma, K. *J. Phys. Chem.* **1996**, *100*, 19357−19363.

(45) Humbel, S.; Sieber, S. N.; Morokuma, K. *J. Chem. Phys.* **1996**, *105*, 1959−1967.

(46) Re, S.; Morokuma, K. *J. Phys. Chem. A* **2001**, *105*, 7185−7197.

(47) Dapprich, S.; Komaromi, I.; Suzie Byun, K.; Morokuma, K.; Frisch, M. J. *J. Mol. Struct.* (*THEOCHEM*) **1999**, *461*, 1−21.

(48) Froese, R. D. J.; Morokuma, K. *Chem. Phys. Lett.* **1999**, *305*, 419−424.

(49) Frisch, M. J.; Trucks, G. W.; Schlegel, H. B.; Scuseria, G. E.; Robb, M. A.; Cheeseman, J. R.; Zakrzewski, V. G.; Montgomery, J. A., Jr.; Stratmann, R. E.; Burant, J. C.; Dapprich, S.; Millam, J. M.; Daniels, D.; Kudin, K. N.; Strain, M. C.; Farkas, O.; Tomasi, J.; Barone, V.; Cossi, M.; Cammi, R.; Mennucci, B.; Pomelli, C.; Adamo, C.; Clifford, S.; Ochterski, J.; Petersson, G. A.; Ayala, P. Y.; Cui, Q.; Morokuma, K.; Malick, D. K.;

Rabuck, A. D.; Raghavachari, K.; Foresman, J. B.; Cioslowski, J.; Ortiz, J. V.; Baboul, A. G.; Stefanov, B.; Liu, G.; Liashenko, A.; Piskorz, P.; Komaromi, I.; Gomperts, R.; Martin, R. L.; Fox, D. J.; Keith, T.; Al-Laham, M. A.; Peng, C. Y.; Nanayakkara, A.; Gonzalez, C.; Chullacombe, M.; Gill, P. M. W.; Johnson, B.; Chen, W.; Wong, M. W.; Andres, J. L.; Head-Gordon, M.; Replogle, E. S.; Pople, J. A. *Gaussian 98*, Revision A.7; Gaussian, Inc.: Pittsburgh, PA, 1998.

(50) Ziegler, T. *Chem. Rev.* **1991**, *91*, 651−667.

(51) Rappe, A. K.; Casewit, C. J.; Colwell, K. S.; Goddard, W. A.; Skiff, W. M. *J. Am. Chem. Soc.* **1992**, *114*, 10024−10035.

(52) Rappe, A. K.; Goddard, W. A. *J. Phys. Chem.* **1991**, *95*, 3358−3363.

(53) Becke, A. D. *J. Chem. Phys.* **1993**, *98*, 1372−1377.

(54) Becke, A. D. *J. Chem. Phys.* **1993**, *98*, 5648−5652.

(55) Becke, A. D. *Phys. Rev. A* **1988**, *38*, 3098−3100.

(56) Lee, C.; Yang, W.; Parr R. G. *Phys. Rev. B* **1988**, *37*, 785−789.

(57) Cheng, H.; Cooper, A. C.; Pez, G. P.; Kostov, M. K.; Piotrowski, P.; Stuart, S. J. *J. Phys. Chem. B* **2005**, *109*, 3780−3786.

(58) Lee, S. M.; An, K. H.; Lee, Y. H.; Seifert, G.; Frauenheim, T. *J. Am. Chem. Soc.* **2001**, *123*, 5059−5063.

(59) Lee, S. M.; Lee, Y. H. *Appl. Phys. Lett.* **2000**, *76*, 2877−2879.

(60) Okmoto, Y.; Miyamoto, Y. *J. Phys. Chem. B* **2001**, *105*, 3470−3474.

(61) Gregg, S. J.; Sing, K. S. W. *Adsorption, Surface Area and Porosity*, 2nd ed.; Academic Press: New York, 1982; pp 111−192.

(62) Cassell, A. M.; Raymakers, J. A.; Kong, J.; Dai, H. *J. Phys. Chem. B* **1999**, *103*, 6484−6492.

(63) Xing, W.; Xue, J. S.; Dahn, J. R. *J. Electrochem. Soc.* **1996**, *143*, 3046−3052.

(64) Buiel, E. R.; George, A. E.; Dahn, J. R. *Carbon* **1999**, *37*, 1399−1407.